Table of Contents

List of Figures

Chapter 1

Glossary

EL Entrainment Layer

ML Mixed Layer

CBL Convective Boundary Layer

LES Large Eddy Simulation

FA Free Atmosphere

GCM General Circulation Model

DNS Direct Numerical Simulation

FFT Fast Fourrier Transform

Chapter 2

Introduction

2.1 Motivation

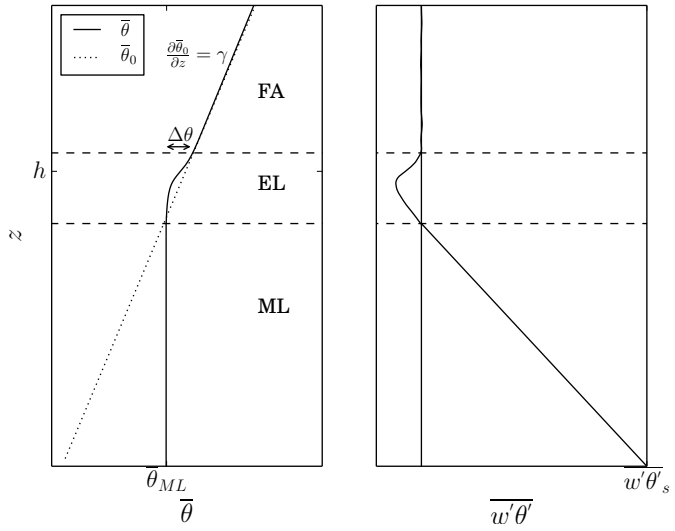

Figure 2.1

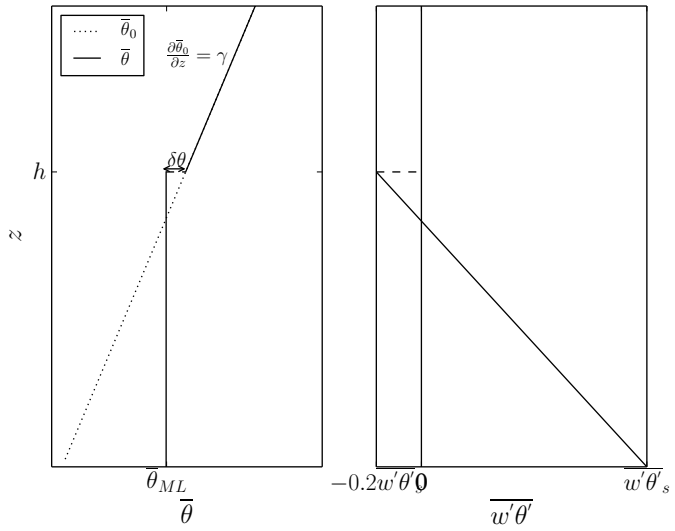

Figure 2.2

2.2 Relevant Background

2.2.1 The Convective Boundary Layer (CBL)

The convective boundary layer over land starts to grow at rapidly at sunrise, peaking at midday. Convective turbulence and the dominant upward vertical motions then begin to subside as the surface cools. In the morning as the surface warms relative to the environment, instability causes thermals to develop and rise with buoyancy driven momentum. They are of uniform potential temperature (θ) and tracer concentration at their cores and entrain surrounding air laterally as they rise, as well as trapping and mixing in stable warm from above. (Stull [13], **?** [**?**])

Under conditions of strong convection, buoyantly driven turbulence dominates and shear is insignificant (**?** [**?**]). Thermals rise, overshoot their natural buoyancy level and overturn or recoil, trapping pockets (or wisps) of warm stable air which then becomes turbulently mixed. This overshoot and

subsequent entrainment of the warmer air from aloft augments the warming caused by the surface heat flux and results in a temperature jump ($\Delta\theta$). A potential temperature (θ) inversion may also be imposed and strengthened for example by subsidence.

Lidar images show the overall structure of the convective boundary layer (CBL) with the rising thermals, impinging on the air above. (**?** [**?**], Traumner et al. [16]) This has been effectively modelled using large eddy simulation (LES) by Schmidt and Schumann in [11]. They used horizontal slices of potential temperature and vertical velocity perturbations ($\theta^{'}$, $w^{'}$) at various vertical levels to show how the thermals form, merge and impinge at the CBL top with concurrent peripheral downward motions. The latter is supported in the visualizations of Sullivan et al. in [15]. Vertical cross sections within the EL show relatively cooler thermal plumes and trapped warmer air as well as the closely associated upward motion of cooler air and downward motion of warmer air.

On average these convective turbulent structures create a mixed layer (ML) with eddy scales cascading from approximately the CBL height (h) to molecular diffusion according to the Kolmagorav power law. Here θ is close to uniform and $\overline{w^{'}\theta^{'}}$ is positive and decreasing. Warming is from both the surface heat flux ($\overline{w^{'}\theta^{'}}_s$) and the flux of entrained stable air at the inversion ($\overline{w^{'}\theta^{'}}_h$). ML turbulence is dominated by warm updraughts and cool downdraughts. With proximity to the top the updraughts become relatively cool and warmer air from above is drawn downward. Above the ML the air becomes more stable with altitude and on average this reflects as a transition from a uniform ML potential temperature ($\frac{\partial\overline{\theta}}{\partial z} \approx 0$) to a stable lapse rate (γ). A peak in the average vertical gradient ($\frac{\partial\overline{\theta}}{\partial z}$) at the inversion represents regions where thermals have exceeded their natural buoyancy level.

Nelson et al. in [10] outline the stages of CBL growth from when the sublayers of the nocturnal boundary layer are entrained, untill the previous day's capping inversion is reached and a quasi-steady state growth is attained.

The EL depth relative to CBL height varies throughout these stages and its relationship to scaled entrainment is hysteresial. Numerical studies typically represent this last quasi-steady phase, since there is usually a constant heat flux working against an inversion and or a stable lapse rate. (Schmidt and Schumann [11], **?** [**?**], Sullivan et al. [15], Evgeni Federovich and Mironov [7], Brooks and Fowler [1])

2.2.2 Convective Boundary Layer Height (h)

The ML is fully turbulent with an on average uniform potential temperature (θ). Aerosol and water vapour concentrations decrease dramatically with transition to the stable upper free atmosphere (FA). So any of these characteristics can support a definition of CBL height (h). Nelson et al. define h in terms of the percentage of ML air and identified it by eye from Lidar back-scatter images in [10]. Traumner et al. compared four automated methods applied to Lidar images: a suitable threshold value above which the air is categorized as ML air, the point of minimum (largest negative) vertical gradient, the point of minimum vertical gradient based on a fitted idealized curve, and the maximum wavelet covariance in [16].

The use of Lidar dominates studies based on measurement. Numerical modelling studies have hundreds of local horizontal points from which smooth averaged vertical profiles be obtained, and statistically robust relationships inferred. Brooks and Fowler [1] applied their wavelet technique to local vertical tracer profiles in their large eddy simulation (LES) study and compared it to the gradient method (i.e. locating the point of minimum vertical gradient) and the point of minimum ($\overline{w'\theta'}$). This last definition has been common in LES and laboratory studies where it's been referred to as the inversion height (J. W. Deardorff and Stockton [9], **?** [**?**], Evgeni Federovich and Mironov [7]). Sullivan et al. [15] clarified that this point does not correspond to the average point of maximum $\frac{\partial\overline{\theta}}{\partial z}$, whereas the upper extrema of the four $\overline{w'\theta'}$ quadrants: upward moving warm air ($\overline{w'^{+}\theta'^{+}}$), downward moving warm air ($\overline{w'^{-}\theta'^{+}}$), upward moving cool air ($\overline{w'^{+}\theta'^{-}}$), downward

moving cool air ($\overline{w'^{-}\theta'^{-}}$) more or less did. They defined CBL height based on local $\frac{\partial\theta}{\partial z}$ and applied horizontal averaging as well as two methods based on $\overline{w'\theta'}$ for comparison.

None of the published LES studies so far define the height in terms of the $\overline{\theta}$ or $\frac{\partial\overline{\theta}}{\partial z}$ profile even though bulk models, from which CBL growth parametrizations stem, rely on an idealized version thereof. Garcia and Mellado do include it as one of their measures of CBL height in their direct numerical simulation study (DNS) [8].

2.2.3 Convective Boundary Layer Growth by Entrainment

In the quasi-steady regime the CBL grows by trapping pockets of warm stable air between or adjacent to impinging thermal plumes. Traumner et al. [16] summarize two relevant buoyancy driven regimes of entrainment:

- Non turbulent fluid can be engulfed between or in the overturning of thermal plumes. This kind of event was seen by Sullivan et al. in [15] when the inversion was weak. Traumner et al.'s observations in [16] support this.
- Impinging thermal plumes distort the inversion interface dragging wisps of warm stable air down at their edges or during recoil under a strong inversion or lapse rate. This type of event is supported by the findings of both Sullivan et al. [15] and Traumner et al. [16].

Under atmospheric conditions shear induced instabilities do occur, and in some laboratory studies under conditions of very high stability the breaking of internal waves have been observed. Both processes are believed to result in some entrainment but we do not consider them here since the former is relatively insignificant in strong convection and the latter has not so far been observed in measurements or modeled output of the atmospheric CBL. (Traumner et al. [16], Sullivan et al. [15])

2.2.4 The Convective Boundary Layer Entrainment Layer

The ML is fully turbulent but the top is characterised by stable air with intermittent turbulence due to the higher reaching thermal plumes. Garcia and Mellado demonstrate that the entrainment layer (EL) is subdivided in terms of length and buoyancy scales. That is, the lower region is comprised of mostly turbulent air with pockets of stable warmer air that are quickly mixed, and so scales with the convective scales (see section 2.4). Whereas the upper region is mostly stable apart from the impinging thermal plumes so scaling here is more influenced by the lapse rate (γ).

In the EL the average vertical heat flux ($\overline{w'\theta'}$) switches sign relative to that in the ML. The fast updraughts are now relatively cool ($\overline{w'^{+}\theta'^{-}}$). In their analysis of the four $\overline{w'\theta'}$ quadrants Sullivan et al. [15] concluded that the overall dynamic in this region is downward motion of warm air from the free atmosphere (FA) ($\overline{w'^{-}\theta'^{+}}$) since the other three quadrants effectively cancel.

In terms of tracer concentration and for example based on a Lidar backscatter profile, there are two ways to conceptually define the entrainment layer (EL). It can be thought of as the range in space (or time) over which local height varies (**?** [**?**]). There is also a local region over which the concentration (or back-scatter intensity) transitions from ML to free atmospheric (FA) values (Traumner et al. [16]). The latter can be estimated using both curve-fitting and wavelet techniques (Traumner et al. [16], Steyn et al. [12], Brooks and Fowler [1]). Traumner et al. [16] compared the two concepts, found them to differ and seem to favour the latter based on how correlated the corresponding scaling relationships were.

Brooks and Fowler apply a wavelet technique to tracer profiles for the determination of EL limits, in their LES study ([1]). But it is more common in numerical modelling and laboratory studies for the EL limits to be defined based on the average vertical heat flux ($\overline{w'\theta'}$) i.e. the point at which it goes from positive to negative values, and the point at which it goes from nega-

tive value to zero (J. W. Deardorff and Stockton [9], Evgeni Federovich and Mironov [7], Garcia and Mellado [8]). Bulk first order models assume the region of negative $\overline{w'\theta'}$ coincides with the region where $\overline{\theta}$ transitions from the ML value to the FA value. (Deardorff [5], [7] [7]). But no modelling studies use the vertical $\overline{\theta}$ profile to define the entrainment layer (EL).

Since the mixed layer $\overline{\theta}$ from a numerical model is not strictly constant (Evgeni Federovich and Mironov [7]), a threshold value for $\overline{\theta}$ or its vertical gradient must be chosen to identify the lower EL limit. Brooks and Fowler encountered inconsistencies when determining the EL limits from the average tracer profile [1]. But the their tracer profile was different to a simulated $\overline{\theta}$ profile whose ML value increases in time predictably based on the $\overline{w'\theta'}$ from the surface and the CBL top or inversion.

2.3 Modelling the Convective Boundary Layer and Entrainment Layer

2.3.1 Bulk Analytical Models

Bulk analytical models for the Convective Boundary layer (CBL) can be subdivided into: (i) zero order and (ii) first order bulk models.

Zero order bulk models assume a Mixed Layer (ML) of uniform potential temperature ($\overline{\theta}_{ML}$) topped by an infinitesimally thin layer across which there is a temperature jump ($\Delta\theta$) and above which is a constant lapse rate (γ). The assumed vertical heat flux ($\overline{w'\theta'}$) profile is linearly decreasing from the surface up, reaching a maximum negative $\overline{w'\theta'}_h$ value which is a constant proportion of the surface value (usually -.2) at the temperature inversion, and decreasing to zero ac-cross the jump. Equations for the evolution of CBL height, $\overline{\theta}_{ML}$ and $\Delta\theta$ are derived on this basis.

For example, if the CBL height (h) is rising, air is being drawn in from the stable layer above and decreasing in enthalpy. So, the decrease in enthalpy

is $c_p \rho \Delta\theta \frac{dh}{dt}$ per unit of horizontal area. Since above the inversion is stable **?** in [**?**] equates this enthalpy loss to the average vertical flux at the inversion.

$$\Delta\theta \frac{dh}{dt} = -\overline{w'\theta'}_h \tag{2.1}$$

The ML warming rate is arrived at via the simplified reynolds averaged conservation of enthalpy

$$\frac{\partial \overline{\theta}_{ML}}{\partial t} = -\frac{\partial}{\partial z} \overline{w'\theta'} \tag{2.2}$$

which based on the assumed constant slope of the vertical heat flux becomes

$$\frac{\partial \overline{\theta}_{ML}}{\partial t} = \frac{\overline{w'\theta'}_s - \overline{w'\theta'}_h}{h} \tag{2.3}$$

and the evolution of the temperature jump ($\Delta\theta$) depends on the rate of CBL height (h) increase, the upper lapse rate γ and the ML warming rate

$$\frac{d\Delta\theta}{dt} = \gamma \frac{dh}{dt} - \frac{d\overline{\theta}_{ML}}{dt} \tag{2.4}$$

An assumption about the vertical heat flux at the inversion (h), such as the entrainment ratio, closes this set.

$$\frac{\overline{w'\theta'}_h}{\overline{w'\theta'}_s} = -.2 \tag{2.5}$$

(**?** [**?**])

The relevant quantities are idealized ensemble averages. There is some variation within this class of model, for example the rate equation for h (entrainment relation) can alternatively be derived based on the turbulent kinetic energy budget (Evgeni Federovich and Mironov [7]). But they are all based on the simplified $\overline{\theta}$ and $\overline{w'\theta'}$ profiles outlined above.

First order models assume an entrainment layer (EL) of finite depth at the top of the ML, defined by two heights: the top of the ML (h_0) and the point

where free atmospheric characteristics are resumed (h_1). The derivations are more complex and examples of simplifying assumptions about the EL are:

- $\Delta h = h_1 - h_0 = Constant$
- Δh or maximum overshoot distance $d \propto \frac{w^*}{N}$ where w^* is the relevant vertical velocity scale and $N = \sqrt{\frac{g}{\overline{\theta}} \frac{\partial \overline{\theta}}{\partial z}}$ is the Brunt-Vaisalla frequency
- and that between h_0 and h_1 $\overline{\theta} = \overline{\theta}_{ML} + f(z,t)\Delta\theta$ where $f(z,t)$ is a dimensionless shape factor

(Deardorff [5], **?** [**?**]).

Although development of these models is beyond the scope of this thesis, mention of them is necessary to give context to the scaling relationships or parametrizations considered.

2.3.2 Numerical Simulations

Numerical simulation of the convective boundary layer (CBL) is carried out by solving the Navier Stokes equations, simplified according to a suitable approximation, on a discrete grid. Types of simulations can be grouped according to the scales of motion they resolve. In direct numerical simulations (DNS) the full range of spatial and temporal turbulence are resolved from the size of the domain down to the smallest dissipative scales i.e. the Kolmagorov micro-scales. This requires a dense numerical grid and so can be computationally prohibitive. In a large eddy simulation (LES) smaller scales are filtered out and parametrized by sub grid scale closure model. General circulation models (GCM) solve the Navier Stokes equations on a spherical grid and parametrize smaller scale processes including convection and cloud cover.

LES has steadily, repeatedly been used to better understand the CBL since Deardorff applied this relatively new method in [4] for this purpose. Sullivan et al. in [15], Evgeni Federovich and Mironov in [7] and Brooks and Fowler in [1] used it to observe the structure and scaling behaviour of the EL.

2.4 Scales of the CBL and Entrainment Layer

2.4.1 Length Scale (h)

Deardorff in [4] demonstrated that the inversion base height scales the sizes of the dominant turbulent structures in penetrative convection. This was taken to be the height of minimum average vertical heat flux (z_f) (J. W. Deardorff and Stockton [9]). Since then, the concept of CBL height (h) has remained reasonably consistent in that it is measured at the inversion or point, above the surface layer, of maximum change in tracer concentration or potential temperature (θ). Turbulence based concepts, such as the velocity variance and the distance over which velocity is correlated with itself, are related but represent the current turbulent dynamics rather than the turbulence history (Traumner et al. [16]).

2.4.2 Convective Velocity Scale (w^*)

Given an average surface vertical heat flux ($\overline{w'\theta'}_s$) a surface buoyancy flux can be defined as $\frac{g}{\theta}\overline{w'\theta'}$ from which the convective velocity scale is obtained by multiplying by the appropriate length scale. Since the result is in $\frac{m^3}{s^3}$ a cube root is applied.

$$w^* = \left(\frac{gh}{\overline{\theta}}\overline{w'\theta'}\right)^{\frac{1}{3}} \tag{2.6}$$

Deardorff ([3]) confirmed that this effectively scaled the vertical turbulent velocity perturbations ($w^{'}$) in the CBL. **?** 's work in [**?**] supports this, even at the CBL top. $\frac{dh}{dt}$ and $w^{'}$ are driven by $\overline{w^{'}\theta^{'}}_s$ and inhibited by γ. The influence of γ on $w^{'}$ is indirectly accounted for via h in w^{*}.

2.4.3 Convective Time Scale (τ)

It logically follows that the time for a thermal to reach the top of the CBL is

$$\tau = \frac{h}{\left(\frac{gh}{\overline{\theta}}\overline{w^{'}\theta^{'}}\right)^{\frac{1}{3}}} \tag{2.7}$$

Sullivan et al. showed a linear relationship between h and time scaled by this time scale in [15]. The time scale associated with the buoyant thermals overshooting and sinking (Brunt-Vaisala frequency) is another obvious choice (Evgeni Federovich and Mironov [7]). The ratio of these two time-scales forms a parameter which characterizes this system. (see **?** [**?**] and Deardorff [5])

2.4.4 Convective Temperature Scale (θ^{*})

The CBL temperature fluctuations $\theta^{'}$ are influenced by $\overline{w^{'}\theta^{'}}$ from both the surface and the CBL top. Deardorff ([3]) showed that an effective scale based on the convective velocity scale is

$$\theta^{*} = \frac{\overline{w^{'}\theta^{'}}}{w^{*}} \tag{2.8}$$

Whereas **?** ([**?**]) showed that as with proximity to the CBL top the effects of γ become more important.

2.4.5 Buoyancy Richardson Number (Ri!)

The flux Richardson (R_f) number expresses the balance between turbulent mechanical energy and buoyancy. It's obtained from the ratio of these two

terms in the turbulent kinetic energy budget equation (Stull [13]):

$$\frac{\partial \overline{e}}{\partial t} + \overline{U}_j \frac{\partial \overline{e}}{\partial x_j} = \delta_{i3} \frac{g}{\overline{\theta}} \left(\overline{u_i' \theta'} \right) - \overline{u_i' u_j'} \frac{\partial \overline{U}_i}{\partial x_j} - \frac{\partial \left(u_j' e' \right)}{\partial x_j} - \frac{1}{\overline{\rho}} \frac{\partial \left(u_i' p' \right)}{\partial x_i} - \epsilon \quad (2.9)$$

$$R_f = \frac{\frac{g}{\overline{\theta}} \left(\overline{w' \theta'} \right)}{\overline{u_i' u_j'} \frac{\partial \overline{U}_i}{\partial x_j}} \quad (2.10)$$

Assuming horizontal homogeneity and neglecting subsidence

$$R_f = \frac{\frac{g}{\overline{\theta}} \left(\overline{w' \theta'} \right)}{\overline{u' w'} \frac{\partial \overline{U}}{\partial z} + \overline{v' w'} \frac{\partial \overline{V}}{\partial z}} \quad (2.11)$$

Applying first order closer to the flux terms, i.e. assuming they are proportional to the vertical gradients, gives the gradient Richardson number (R_g)

$$R_g = \frac{\frac{g}{\overline{\theta}} \frac{\partial \overline{\theta}}{\partial z}}{\left(\frac{\partial \overline{U}}{\partial z} \right)^2 + \left(\frac{\partial \overline{V}}{\partial z} \right)^2} \quad (2.12)$$

which expresses the balance between shear and buoyancy driven turbulence, but in the EL buoyancy acts to suppress buoyancy driven turbulence. Applying a bulk approximation to the denominator, and expressing it in terms of scales yields a ratio of two square of time scales

$$R_g = \frac{\frac{g}{\overline{\theta}} \frac{\partial \overline{\theta}}{\partial z}}{\frac{U^{*2}}{L^2}} = N^2 \frac{L^2}{U^{*2}} \quad (2.13)$$

and applying the bulk approximation to both the numerator and the denominator yields

$$R_b = \frac{\frac{g}{\overline{\theta}} \Delta \theta L}{U^{*2}} \quad (2.14)$$

A natural choice of length and velocity scales for the CBL are h and w^*. Ellison and Turner ([6]) suggested and confirmed a relationship between the

entrainment rate and this form of Richardson number (**Ri!**) based on tank experiments. This parameter can be justified and arrived at by considering the principal forcings of the system, or from non-dimensionalizing the entrainment relation derived analytically (**?** [**?**], Deardorff [4]).

$$w_e \propto \frac{\overline{w'\theta'}_s}{\Delta\theta} \tag{2.15}$$

$$\frac{w_e}{w^*} \propto \frac{\overline{w'\theta'}_s}{\Delta\theta w^*} = Ri^{-1} \tag{2.16}$$

In one or other of its forms this parameter has become central to any study on CBL entrainment (Sullivan et al. [15], Evgeni Federovich and Mironov [7], Traumner et al. [16], Brooks and Fowler [1])

2.4.6 Relationship of Entrainment Rate and Entrainment Layer Depth to Richardson Number

The relationship between scaled entrainment rate and the buoyancy Richardson number (**Ri!**) is arrived at according the zero order bulk model through thermodynamic arguments, or by integration of the conservation of enthalpy or turbulent kinetic energy equations over the growing CBL. (**?** [**?**], Deardorff [5], Evgeni Federovich and Mironov [7]).

$$\frac{w_e}{w^*} \propto Ri^{-a} \tag{2.17}$$

It has been verified in numerous laboratory and numerical studies (J. W. Deardorff and Stockton [9], Sullivan et al. [15], Evgeni Federovich and Mironov [7], Brooks and Fowler [1]). But there is still some unresolved discussion as the the exact value of a. It seems there are two possible values, $-\frac{3}{2}$ and -1, the first of which Ellison and Turner ([6]) suggested occurs at high stability when buoyant recoil of impinging thermals becomes more important than their convective overturning. Evgeni Federovich and Mironov ([7]) arrive at this power law through an **Ri!** obtained using the potential temperature jump across the EL.

A relationship of the scaled entrainment layer EL depth to **Ri!** is arrived at by considering the deceleration of a thermal as it overshoots its natural buoyancy level (Nelson et al. [10]), such that its overshoot distance is

$$d \propto \frac{w^{*2}}{\frac{g}{\overline{\theta}_{ML}}\Delta\theta} \tag{2.18}$$

If the EL depth is proportional to the overshoot distance then

$$\frac{\Delta h}{h} \propto \frac{w^{*2}}{\frac{g}{\overline{\theta}_{ML}}h\Delta\theta} = Ri^{-1} \tag{2.19}$$

? [**?**] integrated the potential and thermal energy difference before and after distortion of the inversion interface with the assumption that the resulting variation in the shape is sinusoidal. He equated this to the total kinetic energy of the CBL and arrived at a $-\frac{1}{2}$ power law relationship

$$\frac{\Delta h}{h} \propto Ri^{-\frac{1}{2}} \tag{2.20}$$

2.5 Research Goals

The LES studies of Sullivan et al. [15], Evgeni Federovich and Mironov [7] and more recently Brooks and Fowler in [1] were primarily carried out on grids of lower vertical resolution than those which at which solutions began to converge in Sullivan and Patton [14]. This strongly influenced our choice of grid size, in particular within the EL

All of the aforementioned were carried out on a $5 \times 5km$ horizontal domain and used a combination of both time and spatial averaging to obtain average profiles. In contrast we chose to run an ensemble of 10 cases each on a smaller domain ($3.2 \times 4.8km$) to obtain true ensemble averages, smoother averaged profiles, and a wealth of local points to make robust basic statistical observations.

Evgeni Federovich and Mironov [7] varied their cases by upper lapse rate

(γ) over a typical range found in the troposphere ($1 - 10K/Km$), whereas Sullivan et al. [15] and Brooks and Fowler in [1] varied surface heat flux and initial inversion ($\Delta\theta$). To obtain a range of Richardson numbers (**Ri!**) we varied what we view to be the two principle parameters of an idealized CBL: surface heat flux ($\overline{w'\theta'}_s$) and upper lapse rate (γ).

2.5.1 Verifying that the Model output is realistic

Since unlike the other LES studies, we initialize with a constant surface heat flux ($\overline{w'\theta'}_s$) working against a constant lapse rate (γ), it is important that we observe the formation of a convective boundary layer (CBL) with the expected average profiles.

Given our concern about a slightly smaller domain than usual, we would like to make sure using visualizations that each of the individual cases are producing coherent turbulent structures and that there is adequate scale separation between the structures with highest energy and the grid size as represented by fast-fourier transforms (FFTs) of the velocity fields.

Sullivan et al. [15] showed with effective visual aids some of the details of the dynamics in the EL. We hope to confirm our large eddy simulation (LES) is producing comparable motions of warm and cool air in this region.

2.5.2 Local Mixed Layer Heights

The average vertical potential temperature ($\overline{\theta}$) profiles correspond to the average of the local vertical θ profiles. The variance in local ML height corresponds to the depth of the average entrainment layer (Δh). Sullivan et al. [15] used a centred differencing gradient method to find the local convective boundary layer (CBL) heights and analyzed the distributions thereof. Brooks and Fowler in [1] applied a wavelet of dilation comparable to EL depth to local tracer profiles to determine the location of the EL and then

a narrower wavelet to determine the limits. They subsequently applied horizontal and time averaging.

Since the local profiles are not smooth, and there is often upper variability of similar and greater magnitude than that which separates the mixed layer (ML) from the layer above, the gradient method is not reliable. A typical tracer profile is quite different to a θ profile in that it goes from a large value in the CBL to a much lower value above. So it can be effectively idealized by a step function. The vertical potential temperature gradient ($\frac{\partial\theta}{\partial z}$) profile in this study could be approximated by a step function. But given the possible magnitude of upper variability relative to that across the EL, a wavelet technique might not be as well suited.

Steyn et al. in [12] fitted an idealized curve to tracer profiles (Lidar backscatter). So we apply this idea and the multi-linear regression method outlined by Vieth in [18] to our local θ profiles. The result is a three line fit, one line for each of the layers: the ML of almost constant θ, the EL over which transition to the stable layer above occurs, and the stable layer of constant lapse rate γ. From this the local height of the mixed layer (ML) can readily be determined and the distribution of local ML heights (h_0^l) should correspond to the concept of the EL.

We would expect increased stability (γ) to reduce the distortion of the inversion interface and so the variation in h_0^l. Increased surface heat flux ($w^{'}\theta_s^{'}$) would increase the overall magnitude of h_0^l. We will use histograms to simply represent these expected effects. The h_0^l surface should correspond to coherent regions of warm and cool air. In particular height h_0^l should correspond to impinging relatively cool thermals at the top of the EL. We will use 2-d snapshots of $w^{'}$, $\theta^{'}$ and the h_0^l surface to demonstrate this.

2.5.3 Flux Quadrants

Since the average potential temperature profile ($\overline{\theta}$) represents the results of warming, and warming occurs via the flux of heat from below and above ($\overline{w'\theta'}_s$, $\overline{w'\theta'}_h$) observation and analysis of the heat flux ($w'\theta'$)s should shed light on the shape of vertical ($\overline{\theta}$) profile. For instance the upper lapse rate (γ) surely influences the downward moving warm air ($\overline{w'^{-}\theta'^{+}}$) in the the EL and so the heating rate from above of the ML.

Quadrant analysis have been carried out on the vertical heat flux from both LES output and measurement (Sullivan et al., [15] and **?** , [**?**]). The effects of upper lapse rate (γ) on temperature and velocity perturbations in the CBL were analyzed by **?** in [**?**]. Following these three studies we break the $\overline{w'\theta'}$ into four quadrants to see the vertical average individual profiles and also the joint distributions at the EL limits and the inversion (h). In particular to isolate the effects of γ we will scale by the convective velocity and temperature variance scales w^* and $\theta^* = \frac{\overline{w'\theta'}_s}{w^*}$.

2.5.4 Choice of Height Definitions

Bulk models assume that the region of transition from the ML value to the free atmospheric (FA) value in the vertical $\overline{\theta}$ profile corresponds to the region of negative $\overline{w'\theta'}$ (Deardorff [5], Evgeni Federovich and Mironov [7]). Although the height of maximum $\frac{\partial\overline{\theta}}{\partial z}$ or average of local heights of $\frac{\partial\theta}{\partial z}$ is used as a measure of CBL height (Sullivan et al., [15] and Garcia and Mellado [8]) there does not seem to be an example in the literature where the EL limits are defined in terms of the vertical $\overline{\theta}$ profile.

So here, we test this framework in terms of two relevant parametrizations. That is we define both the CBL height and EL limits in terms of the vertical $\frac{\partial\overline{\theta}}{\partial z}$ profile. It follows that the temperature jump ($\Delta\theta$) is defined as the difference across the EL. This is a first order type framework. We approximate the zero order framework by defining the θ jump as the difference between the ML value and the value at h on the initial vertical $\overline{\theta}$ profile.

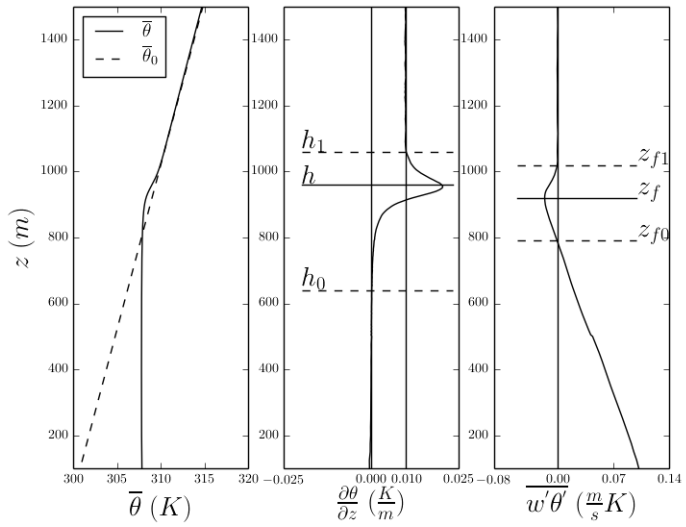

Figure 2.3: Height Definitions

CBL Height	ML $\overline{\theta}$	EL Limits	θ Jump	**Ri!**
h (see Figure 2.3)	$\overline{\theta}_{ML} = \frac{1}{h}\int_0^h \overline{\theta}(z)dz$	h_0, h_1	$\delta\theta = \overline{\theta}(h_1) - \overline{\theta}(h_0)$	**Ri!** $= \frac{\delta\theta}{\frac{\overline{w'\theta'}_s}{w^*}}$
			$\Delta\theta = \overline{\theta}_0(h) - \overline{\theta}_{ML}$	**Ri!**$= \frac{\Delta\theta}{\frac{\overline{w'\theta'}_s}{w^*}}$

Table 2.1: Relevant Definitions used in this Study

2.5.5 $\frac{w_e}{w^*}$ vs Ri

The relationship of scaled entrainment velocity to the buoyancy Richardson number (**Ri!**) is well established (Deardorff [5] J. W. Deardorff and Stockton, [9], Stull [13]).

$$\frac{w_e}{w^*} \propto Ri^{-a} \tag{2.21}$$

This relationship, in particular when $a = 1$, is based on a simplified zero order framework so strictly the length-scale and $\Delta\theta$ should be defined accordingly. We will test this relationship under our zero and 1st order frameworks. We will further define the three principal heights in terms of the vertical $\overline{w'\theta'}$ profile to enable comparison with other similar numerical studies.

There is some discussion in the literature about the power exponent of the Richardson number (**Ri!**) and it seems the two major contenders are -1 and $-\frac{3}{2}$. The latter has been discussed in the context of a shift in entrainment mechanism from eddy turnover to recoil at higher **Ri!** (Turner [17]), under conditions of a large upper lapse rate (γ) J. W. Deardorff and Stockton [9]. Evgeni Federovich and Mironov [7] assert that it is inferred when the first order **Ri!** is used and the temperature jump is taken across the EL. Whereas Sullivan et al. in [15] speculate a power law other than -1 may apply at lower **Ri!**. We will plot our data in log-log coordinates to observe which if any power law applies to our results.

2.5.6 $\frac{\Delta h}{h}$ vs Ri

Relationship of the scaled EL depth to **Ri!** arises from a momentum balance where the depth is considered to be related to the overshoot of the convective thermals (**?** [**?**], J. W. Deardorff and Stockton [9]). This in turn is a function of the velocity at the top of the CBL and the buoyancy difference across it. When the velocity at the top is assumed to be proportional the the convective velocity scale (w^*) this becomes

$$\frac{\Delta h}{h} \propto Ri^{-1} \tag{2.22}$$

? in [**?**] arrived at a $-\frac{1}{2}$ power law relationship using an energy balance. He equated the difference in potential and thermal energy before and after distortion of the inversion interface to the kinetic energy before distortion. Model output, laboratory and field measurements have resulted in power laws ranging from -1 to $-\frac{1}{4}$ (Traumner et al. [16]).

Given that our definition of the EL has not been used before we will first check for a relationship of scaled depth ($\frac{\Delta h}{h}$) to **Ri!**. Once that is established, we will use log-log coordinates to see which power law best fits.

Bibliography

[] R. Boers. A parametrization of the depth of the entrainment zone. *Journal of Applied Meteorology*, pages 107–111, 1989. → pages

[1] I. M. Brooks and A. M. Fowler. An evaluation of boundary-layer depth, inversion and entrainment parameters by large-eddy simulation. *Bundary-Layer Meteorology*, 142:245–263, 2012. → pages

[] T. D. Crum, R. B. Stull, and E. W. Eloranta. Coincident lidar and aircraft observations of entrainment into thermals and mixed layers. *Journal of Climate and Applied Meteorology*, 26:774–788, 1987. → pages

[3] J. W. Deardorff. Convective velocity and temperature scales for the unstable planetary boundary layer and for rayleigh convection. *Journal of the Atmospheric Sciences*, 27:1211 – 1213, 1970. → pages

[4] J. W. Deardorff. Numerical investigation of neutral and unstable planetary boundary layers. *Journal of the Atmospheric Sciences*, 29: 91 – 115, 1972. → pages

[5] J. W. Deardorff. Prediction of convective mixed-layer entrainment for realistic capping inversion structure. *Journal of the Atmospheric Sciences*, 36:424–436, 1979. → pages

[9] J. W. Deardorff, G. E. Willis, and B. J. Stockton. Laboratory studies of the entrainment zone of a convectively mixed layer. *J. Fluid Mech.*, 100:41–64, 1980. → pages

[6] T. H. Ellison and J. S. Turner. Turbulent entrainment in stratified flows. *Journal of Fluid Mechanics*, 6:423–448, 1959. → pages

[7] E. Federovich, R. Conzemus, and D. Mironov. Convective entrainmnent into a shear-free, linearly stratifies atmosphere: Bulk

models reevaluated through large eddie simulation. *Journal of the Atmospheric Sciences*, 61:281 – 295, 2004. → pages

[] E. Fedorovich and R. Conzemius. *Large Eddy Simulation of Convective Entrainment in Linearly and Discretely Stratified Fluids*. Kluwer Academic Publishers, 1 edition, 2001. → pages

[8] J. R. Garcia and J. P. Mellado. The two-layer structure of the entrainment zone in the convective boundary layer. *Journal of the Atmospheric Sciences*, 2014. doi:10.1175/JAS-D-130148.1. → pages

[] L. Mahrt and J. Paumier. Heat transport in the atmospheric boundary layer. *Journal of the Atmospheric Sciences*, 41:3061–3075, 1984. → pages

[10] E. Nelson, R. Stull, and E. Eloranta. A prognostic relationship for entrainment zone thickness. *Journal of Applied Meteorology*, 28: 885–901, 1989. → pages

[11] H. Schmidt and U. Schumann. Coherent structure of the convective boundary layer derived from larg-eddy simulations. *J. Fluid. Mech.*, 200:511–562, 1989. → pages

[] Z. Sorbjan. Effects caused by varying the strenth of the capping inversion based on a large eddie simulation of the shear free convective boundary layer. *Journal of the Atmospheric Sciences*, 53:2015 – 2023, 1996. → pages

[] Z. Sorbjan. Similarity of scalar fields in the convective boundary layer. *Journal of the Atmospheric Sciences*, 56:2212 – 2221, 1999. → pages

[12] D. G. Steyn, M. Baldi, and R. M. Hoff. The detection of mixed layer depth and entrainment zone thickness from lidar backscatter profiles. *Journal of Atmospheric and Oceanic Technology*, 16:953–959, 1999. → pages

[] R. Stull. Inversion rise model based on penetrative convection. *Journal of the Atmospheric Sciences*, 30:1092–1099, 1973. → pages

[13] R. Stull. *An Introduction to Boundary Layer Meteorology*. Kluwer Academic Publishers, 1 edition, 1988. ISBN 9027727686. → pages

[14] P. P. Sullivan and E. G. Patton. The effect of mesh resolution on convective boundary layer statistics and structures generated by large

eddie simulation. *Journal of the Atmospheric Sciences*, 58:2395–2415, 2011. doi:10.1175/JAS-D-10-05010.1. → pages

[15] P. P. Sullivan, C.-H. Moeng, B. Stevens, D. H. Lenschow, and S. D. Mayor. Structure of the entrainment zone capping the convective atmospheric boundary layer. *Journal of the Atmospheric Sciences*, 55: 3042–3063, 1998. doi:10.1007/s10546-011-9668-3. → pages

[] H. Tennekes. A model for the dynamics of the inversion above a convective boundary layer. *Journal of the Atmospheric Sciences*, 30: 558–566, 1973. → pages

[16] K. Traumner, C. Kottmeier, U. Corsmeier, and A. Wieser. Convective boundary-layer entrainment: Short review and progress using doppler lidar. *Bundary-Layer Meteorology*, 141:369–391, 2011. doi:10.1007/s10546-011-9657-6. → pages

[17] J. S. Turner. Turbulent entrainment: the development of the entrainment assumption and its application to geophysical flows. *J. Fluid Mech.*, 173:431–471, 1986. → pages

[18] E. Vieth. Fitting piecewise linear regression functions to biological responses. *Journal of Applied Physiology*, 67:390–396, 2011. → pages